RESEARCH ARTICLE

Key Points:
- Illumination of the micromechanical processes that control frictional healing
- Investigation of the role of water in the evolution of contact junctions
- Physicochemical processes determine fault strength and stress drop

Physicochemical processes of frictional healing: Effects of water on stick-slip stress drop and friction of granular fault gouge

Marco M. Scuderi[1], Brett M. Carpenter[1,2], and Chris Marone[1]

[1]Department of Geosciences, Pennsylvania State University, University Park, Pennsylvania, USA, [2]Istituto Nazionale di Geofisica e Vulcanologia, Rome, Italy

Abstract Understanding the micromechanical processes that dictate the evolution of fault strength during the seismic cycle is a fundamental problem in earthquake physics. We report on laboratory experiments that investigate the role of water during repetitive stick-slip frictional sliding, with particular emphasis on the grain-scale and atomic-scale mechanisms of frictional restrengthening (healing). Our experiments are designed to test underlying concepts of rate and state friction laws. We sheared layers of soda-lime glass beads in a double direct shear configuration at a constant normal stress of 5 MPa. Shear stress was applied via a constant displacement rate from 0.3 to 300 µm/s. During each experiment, relative air humidity (RH) was kept constant at values of 5, 50, or 100%. Our data show a systematic increase in maximum friction (μ_{max}), stick-slip friction drop ($\Delta\mu$), and frictional healing rate, with increasing RH. The highest values of interevent dilation occur at 100% RH. Postexperiment scanning electron microscope observations reveal details of contact junction processes, showing a larger grain-to-grain contact area at higher RH. We find that the evolution of contact area depends inversely on slip velocity and directly on RH. Our results illuminate the fundamental processes that dictate stick-slip frictional sliding and provide important constraints on the mechanisms of rate and state friction.

1. Introduction

Understanding the processes that dictate the evolution of frictional strength during the seismic cycle is a central problem in characterizing the seismic potential of faults and in relating earthquake source parameters such as stress drop to recurrence interval and geologic and geodetic fault slip rates. Seismological observations indicate that faults restrengthen during the interseismic period, and existing work documents a systematic variation in stress drop and other source parameters with earthquake recurrence interval [e.g., *Kanamori and Allen*, 1986; *Scholz et al.*, 1986; *Vidale et al.*, 1994; *Marone et al.*, 1995; *Schaff et al.*, 1998; *Scholz*, 2002]. Estimates based on seismic moment show that stress drop generally increases by a few megapascal per decade increase in earthquake recurrence time [e.g., *Scholz et al.*, 1986]; however, more complex relationships are also observed, including decreasing stress drop with recurrence interval [e.g.,*Peng et al.*, 2005].

Laboratory friction experiments provide insight into the mechanisms of fault healing, and results of these studies provide the fundamental underpinnings of the rate and state friction laws. Existing works show that static friction increases logarithmically with contact time, although a power law relationship is often permissible, and stick-slip recurrence interval [e.g., *Dieterich*, 1972, 1978; *Bos et al.*, 2000; *Losert et al.*, 2000; *Frye and Marone*, 2002a, 2002b; *Mair et al.*, 2002; *Tenthorey and Cox*, 2006; *Niemeijer et al.*, 2008; (B. M. Carpenter et al., Variation in mechanical behavior of a carbonate-bearing normal fault: Monte Maggio fault, submitted to *Journal of Geophysics Research*, 2014)]. Frictional healing is the mechanism associated with fault restrengthening following failure, where time-, slip-, and velocity-dependent processes dictate the evolution of real contact area at grain junctions, in granular material, or at asperity contacts on extended solid surfaces [*Rabinowicz*, 1951; *Dieterich*, 1972, 1978, 1979; *Scholz and Engelder*, 1976; *Teufel and Logan*, 1978; *Ruina*, 1983; *Dieterich and Conrad*, 1984; *Tullis and Weeks*, 1986; *Chester*, 1994; *Dieterich and Kilgore*, 1994; *Marone*, 1998]. However, the atomic-scale mechanisms that dictate frictional restrengthening in fault rocks are poorly understood. Presumably, physicochemical processes acting at highly stressed contact junctions between grains [e.g., *Rabinowicz*, 1951] dictate the evolution of frictional strength, via the size or quality of contact area [e.g., *Tullis*, 1988; *Li et al.*, 2011]; however, the details of these processes are unclear under even simple boundary conditions, not to mention during repetitive stick slip on tectonic faults subject to continuous shear.

Numerical simulations [*Mora and Place*, 1994, 1998, 1999; *Morgan*, 1999; *Morgan and Boettcher*, 1999; *Guo and Morgan*, 2004, 2006; *Abe and Mair*, 2005, 2009; *Mair and Abe*, 2008, 2011; *Rathbun et al.*, 2013] and laboratory experiments [*Mair et al.*, 2002; *Frye and Marone*, 2002a; *Anthony and Marone*, 2005; *Yasuhara et al.*, 2005; *Marone et al.*, 2008] on granular fault gouge have shown that gouge material (angular versus spherical particles and narrow versus wide particle size distribution) and micromechanical deformation (grain comminution, dilation, shear localization, sliding, and/or rolling) control the evolution of the real contact area, and as a consequence, frictional strength, and stability. Water also plays a fundamental role in determining the time-dependent deformation at grain contact junctions [*Dieterich and Conrad*, 1984; *Losert et al.*, 2000; *Frye and Marone*, 2002b; *Renard et al.*, 2012]. Hydrolytic weakening has been proposed as a possible mechanism for plastic deformation at grain contact junctions by which the real contact area grows with time, resulting in an overall increase of frictional strength [*Griggs and Blacic*, 1965; *Blacic and Christie*, 1984; *Frye and Marone*, 2002b]. Pressure dissolution, diffusion, and precipitation have also been proposed as a series of linked processes capable of inducing plastic deformation at grain contact junctions, driving compaction, and reducing pore space in silica aggregates [*Bos and Spiers*, 2002; *Niemeijer et al.*, 2002; *Yasuhara et al.*, 2003, 2005; *Zhang and Spiers*, 2005; *Niemeijer et al.*, 2010; *Visser et al.*, 2012; *Zheng and Elsworth*, 2012, 2013]. Other possible water-assisted mechanisms that can result in healing, such as capillary bridging, subcritical crack growth, and adsorption/desorption, may also promote time-dependent plastic deformation at grain junctions.

Dieterich and Conrad [1984] showed that for bare quartzite surfaces, dry conditions resulted in higher friction and more stable sliding than humid conditions. They suggested that water acted as a lubricant, weakening contact junctions, yet increasing the rate of frictional healing and thus promoting stick-slip instability. *Frye and Marone* [2002b] studied granular friction and also found that the rate of frictional healing increased with increasing relative humidity (RH). However, in contrast to the results for bare surfaces [*Dieterich and Conrad*, 1984], they found (1) that sliding friction is independent of RH and (2) that a transition occurs from velocity strengthening frictional behavior to velocity weakening frictional behavior above a critical RH of 30–35%. Both of these studies imply that chemically assisted, thermally activated mechanisms related to the adsorption of water promote plastic deformation at asperity contacts. This suggests that the real contact area grows with time, resulting in an increase in frictional strength [*Renard et al.*, 2012]. However, relatively little is known about the role of water at asperity contacts during the deformation of a dynamic system (i.e., repetitive frictional stick slip) and its control on the relationships between aseismic creep, recurrence time, and stress drop magnitude.

The purpose of this paper is to investigate the effect of water-activated mechanisms on contact morphology, frictional healing, and dynamic instabilities within granular fault gouge during stick-slip frictional sliding as an analog for the seismic cycle [*Brace and Byerlee*, 1966]. We focus on the time and slip dependence of friction during repetitive stick slip in experiments, for which the sliding rate and relative humidity were varied systematically.

2. Experimental Methods

We performed experiments on synthetic granular fault gouge composed of glass beads using a fast acting, servohydraulic, biaxial deformation apparatus in a double direct shear configuration under conditions of room temperature and controlled humidity (Figure 1a). A horizontal ram applies and maintains a constant force normal to the shearing layer in load feedback control, and shear load is applied as a constant shear displacement rate via a vertical ram. The applied loads (both vertical and horizontal) are measured using custom-built, strain gauge load cells with an amplified output of ±5 V and an accuracy of ±0.5 N. Shear and normal displacements are measured using direct current displacement transducers (DCDT), positioned between the fixed frame and the moving pistons, with an accuracy of ±0.1 µm. A stiffness correction for stretch of the apparatus is applied, with nominal values of 0.5 kN/µm for the vertical frame and 0.37 kN/µm for the horizontal frame. Data were recorded with a 24 bit ±10 V analog to digital converter at a rate of 10 kHz and averaged to obtain sampling rates between 1 Hz and 10 kHz.

2.1. Sample Configuration and Starting Material

Gouge layers were composed of smooth, soda-lime glass beads GL-0191, Mo-Sci Corporation, Rolla, Missouri (Figure 1c). Bead particle size ranged from 105 to 149 µm in diameter, and the chemical composition (by weight) was silica 65–75%, sodium oxide 10–20%, calcium oxide 6–15%, magnesium oxide 1–5%, and aluminum oxide 0–5%. Glass beads are widely used as a laboratory analog for granular fault gouge [e.g., *Losert et al.*, 2000; *Mair*
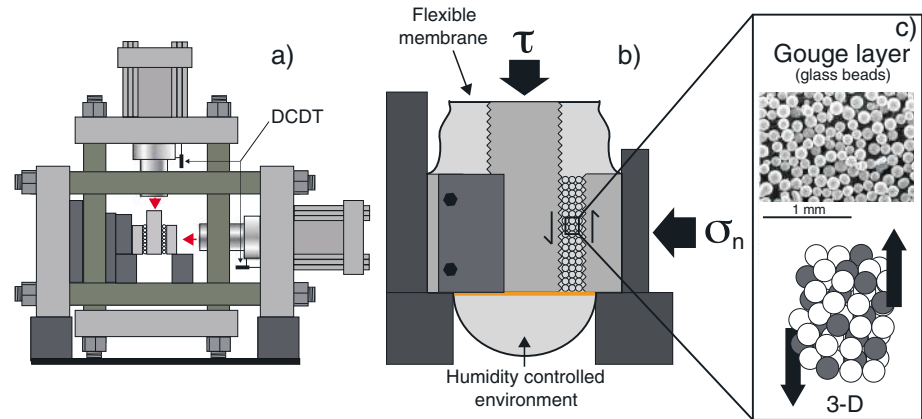
Figure 1. (a) Biaxial deformation apparatus and double direct shear configuration. The horizontal ram applies a constant normal force, and the vertical ram drives shear at a controlled displacement rate. Normal and shear displacement are measured via DCDTs mounted on each ram. (b) Sample assembly composed of two gouge layers sandwiched between two stationary side blocks and a central forcing block, each with grooves perpendicular to shear direction to inhibit boundary shear. Guide plates are attached to the side blocks, and a thin latex membrane covers the layer bottom. A sealed plastic membrane is used to control relative humidity around the sample. (c) Starting material: (top) SEM image of glass beads before shearing. (bottom) Schematic of the granular particles and associated sense of shear.

et al., 2002; *Johnson et al.*, 2008, 2013]. Previous work shows that glass beads exhibit highly reproducible stick-slip frictional sliding [e.g., *Mair et al.*, 2002; *Savage and Marone*, 2007, 2008]. This material also allows us to accurately analyze the resulting postexperiment grain morphology.

The double direct shear sample configuration consisted of a three-block assembly with a central forcing block and two stationary side blocks (Figure 1b). The forcing blocks are constructed from hardened steel and equipped with grooves, 0.8 mm in height and 1 mm spacing, on the surfaces in contact with the gouge perpendicular to shear direction. The side blocks have nominal frictional contact area of $10 \times 10 \, cm^2$, and the central block has dimensions of $15 \times 10 \times 4 \, cm$, such that frictional contact area remains constant during shear. Two identical granular layers are sheared simultaneously in double direct shear. All measurements given in this paper are for a single layer.

Table 1. Experiment List and Boundary Conditions[a]

Experiment Number	Shear Velocity (μm/s)	Relative Humidity (RH%)
p3476	0.3–300	5
p3331	0.3–300	5
p3332	0.3–300	5
p3359	0.3–300	50
p3316	0.3–300	50
p3317	0.3 - 300	50
p3368	0.3–300	100
p3444	0.3–300	100
p3445	0.3 - 300	100
p3448	300 - 0.3	5
p3479	300–0.3	5
p3480	300–0.3	5
p3580	300–0.3	50
p3581	300–0.3	50
p3447	300–0.3	100
p3619	300–0.3	100
p3618	300–0.3	100

[a]All experiments were done with a constant normal stress of 5 MPa and an initial gouge layer thickness of 5 mm.

Gouge layers were constructed using a precise leveling jig in order to obtain a uniform and reproducible layer thickness of 5 mm [e.g., *Anthony and Marone*, 2005]. Cellophane tape was used to confine the layers during sample construction, which consisted of placing the central block on top of the side block, securing it with additional tape, and then repeating the procedure for the other side block. Subsequently, a thin latex membrane was attached to the bottom of the sample to avoid loss of material during the experiment, and four steel guide platens were secured on each side of the sample to avoid lateral extrusion of the material (Figure 1b).

2.2. Experimental Procedure

Experiments were conducted using three different values of relative humidity for the air in contact with the gouge layer: ~5%, 50%, and 100% (Table 1). In order to eliminate moisture,
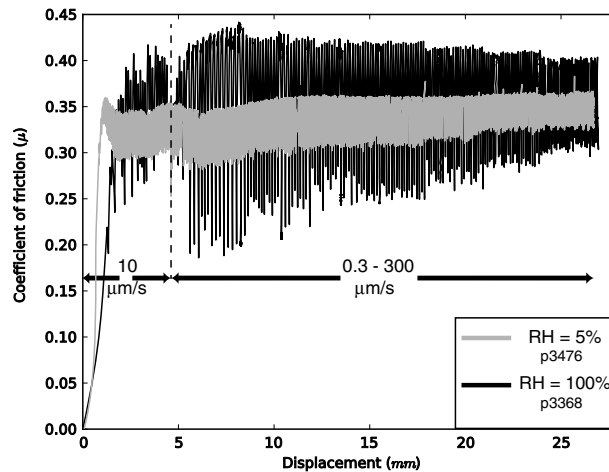
Figure 2. Complete run details showing coefficient of friction versus shear displacement for two representative experiments: one at 5% RH (p3476) and one at 100% RH (p3368). Samples are sheared at a constant displacement rate of 10 μm/s for 5 mm after which velocity step tests are performed for the range 0.3 to 300 μm/s. Both experiments show repetitive stick-slip instabilities. Friction drops are much larger (up to 0.2) at 100% RH than under drier conditions at 5% RH. For both experiments, friction drop decreases as shear velocity increases.

gouge particles were dried in an oven for 24 h at 100°C prior to sample construction. Subsequently, the sample was quickly assembled, following the procedure described above, and placed in a controlled humidity environment for an additional 24 h at the desired RH. Nominally dry conditions (RH ≈ 5%) were achieved by using an anhydrous calcium sulfate desiccant (W.A. Hammond Drierite Company, Ltd.). Experiments at 50% RH were done during the months between June and August, as ambient weather conditions permitted. Experiments at 100% RH were done using a solution of anhydrous sodium carbonate (Na_2CO_3) and deionized water (1:2).

After the sample was constructed, it was placed in a flexible, sealed membrane within the deformation apparatus (Figures 1a and 1b). We maintained constant RH within the membrane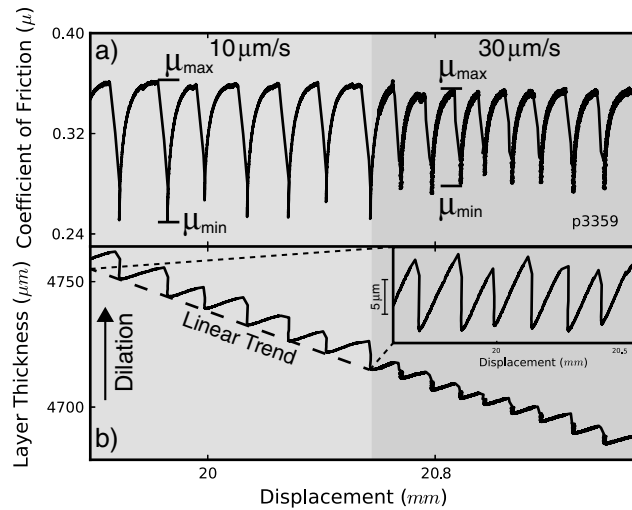 throughout the experiment. Once the system had equilibrated, normal stress (σ_n) was raised to 5 MPa and maintained constant. All experiments were run in the nonfracture loading regime for glass beads [*Mair et al.*, 2002; *Mair and Abe*, 2011]. Once initial compaction stabilized to a constant layer thickness, the vertical piston was driven down at a constant displacement rate of 10 μm/s for ~5 mm allowing friction to increase, generally to a peak value, after which stick-slip events stabilize within a constant range (Figure 2). The load point velocity was then increased stepwise from 0.3 to 300 μm/s (Figure 2). To investigate time- and strain-dependent frictional evolution, experiments were also performed with the reverse velocity sequence, from 300 to 0.3 μm/s, under the same boundary conditions (Table 1). For a given boundary condition, each experiment was repeated at least 3 times, and we observed a very high level of reproducibility (Table 1). At the end of each experiment, the sample assembly was carefully removed, and the gouge layers were collected for postexperiment analysis via optical and scanning electron microscope (SEM).

3. Results

3.1. Characteristics of Laboratory Stick-Slip Events

Experiments were conducted using a computer-controlled displacement history. During the first stage of loading, at constant velocity of 10 μm/s, shear stress increased linearly during elastic loading to an inelastic yield point, followed by a peak yield strength, after which stick-slip instabilities began (Figure 2). Frictional strength evolved during the initial period of stick slip and reached a mechanical steady state, defined by constant maximum and minimum values of friction (Figure 2). Under dry conditions of 5% RH, layers exhibited higher elastic stiffness and lower peak strength than under humid conditions (RH = 100%).

After friction had reached a mechanical steady state (i.e., constant μ_{max} and μ_{min}), we performed velocity step tests to assess the time-dependent evolution of friction (Figure 2). Upon an increase in loading velocity, we find a marked decrease of friction drop ($\Delta\mu = \mu_{max} - \mu_{min}$) and an increase in stick-slip event frequency (Figure 3a). Consistent with previous works, our results show that the magnitude of friction drop, layer thickness change (Δh), and interevent recurrence time, t_n, vary systematically with loading velocity (Figure 3) [*Mair et al.*, 2002; *Anthony and Marone*, 2005].

Stick-slip events are characterized by a typical, three-stage history (Figure 4). (1) Initially, friction ($\mu = \tau/\sigma_n$) increases linearly during elastic loading, characterized by stiffness in the form $k' = k/\sigma_n$ (μm^{-1}), where k (N/μm) represents elastic stiffness given by the ratio of shear stress (τ) to shear displacement, and σ_n is the applied

Figure 3. Details of an experiment (p3359) at 50% RH showing friction (μ) and layer thickness versus shear displacement. (a) Stick-slip friction drop decreases as shear velocity increases. (b) Evolution of gouge layer thickness with shear. Note that dilation occurs during stress buildup, and compaction occurs upon failure and stress drop. Inset shows layer thickness data for the 10 µm/s section after removing linear trend for geometric thinning.
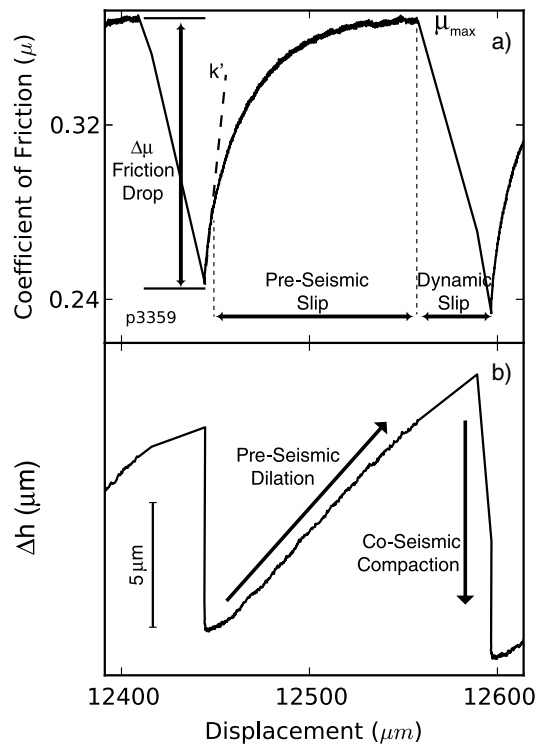

Figure 4. (a) Details of the friction coefficient for a stick-slip event. The $\Delta\mu$ is the dynamic friction drop upon stick-slip failure. Shear stress increases linearly during elastic loading, given by $k' = k/\sigma_n$, where k is the stiffness of the apparatus given as shear stress per shear displacement. Deviation from linear elastic loading marks the onset of inelastic slip until a maximum strength (μ_{max}) and failure. (b) Evolution of layer thickness for the same stick-slip event. Gouge layers dilate during inelastic creep and then abruptly compact upon dynamic failure.

normal stress (Figure 4a). During this phase, layer thickness experiences minor changes, suggesting elastic deformation at grain-to-grain contacts (Figure 4b) [e.g., *Anthony and Marone*, 2005]. (2) Deviation from linear elastic loading marks the onset of plastic strain, which is associated with gouge layer dilation and elastoplastic deformation at grain contacts (Figure 4). (3) When the maximum frictional strength (μ_{max}) is reached, dynamic failure and slip occurs with an associated friction drop ($\Delta\mu$) and abrupt compaction of the gouge layer.

During a series of multiple stick-slip events, layer thickness shows a strong correlation with the magnitude of friction drop and shear velocity (Figures 3a and 3b). At a constant loading rate, the amount of preseismic dilation and coseismic compaction is constant and does not vary substantially with net shear strain.

In response to an increase in velocity, stick-slip stress drop decreases and the relative amount of prefailure dilation (Δh) and dynamic compaction decreases (Figure 3). When analyzing the evolution of layer thickness, we corrected the measurements from the DCDT (Figure 1a) to account for geometrical layer thinning due to sample geometry [*Scott et al.*, 1994; *Samuelson et al.*, 2009]. We removed a linear trend from the layer thickness data to account for overall thinning (Figure 3b), so that we could accurately determine layer thickness changes during a given stick-slip event (Figure 3b inset).

Loading rate has a systematic effect on stick-slip recurrence time. Consistent with previous work, we find a power law relationship of the form $\log(t_r) = m\log(v)$, with $m\sim-1.1$, resulting in longer interevent times at slower velocities (Figure 5 inset) [*Karner and Marone*, 2000; *Mair et al.*, 2002; *Anthony and Marone*, 2005; *Savage and Marone*, 2007]. For each loading velocity, we analyzed every stick-slip event, reporting the mean value and statistical variability, with error bars calculated by using a standard error
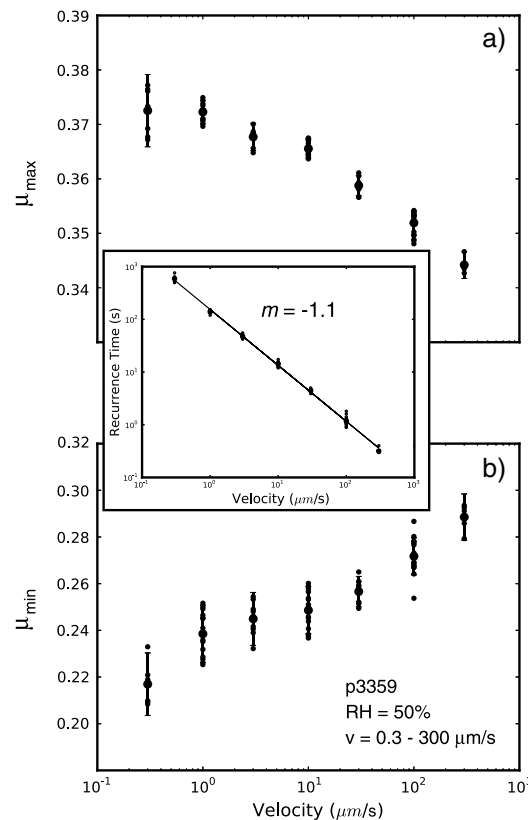
Figure 5. Stick-slip friction parameters for an experiment at 50% RH (p3359). (a) Peak friction μ_{max}, (b) minimum friction μ_{min}, and stick-slip recurrence interval t_r (inset) as a function of shearing velocity. Figures 5a and 5b show all data for one experiment and mean values. Note that μ_{max} decreases systematically and μ_{min} increases systematically as velocity increases. Recurrence interval decreases as loading velocity increases (inset).

of the mean method (Figure 5). For our range of velocities, μ_{max} decreased (Figure 5a) and μ_{min} increased (Figure 5b) with the logarithm of shear velocity. Note that both of these trends change slightly at 10 µm/s (Figure 5).

3.2. Effect of Shear Velocity and Humidity on Friction Drop

We find systematic variation in stick-slip properties as a function of relative humidity, shear velocity, and loading history (i.e., slow-to-fast and fast-to-slow velocity sequences) (Figure 6). For a given shear velocity, as humidity increases, μ_{max} increases and μ_{min} decreases, resulting in systematic changes in $\Delta\mu$ (Figure 6). For the dry experiments, μ_{max} is fairly insensitive to loading rate, within the scatter in the data, although μ_{min} varies systematically, resulting in roughly constant values of $\Delta\mu$ below 10 µm/s and a decrease in $\Delta\mu$ with velocity above 10 µm/s.

For experiments at 50% and 100% RH, loading history has a significant influence on μ_{max} and μ_{min}. For the velocity step sequence from 0.3 to 300 µm/s, μ_{max} is always higher when compared to the inverted sequence (from 300 to 0.3 µm/s). However, this relation is not observed in dry experiments. The effect of loading history on μ_{min} is more complex. Data collected under humid conditions, 50% and 100% RH, show lower friction values with increasing velocity (0.3 to 300 µm/s) than for the reverse velocity history, whereas the opposite is true for dry conditions (Figure 6). Two general observations can be made. First, the stick-slip parameter μ_{min} shows a more consistent variation with loading velocity under dry conditions when compared to wet conditions,

whereas the opposite is true for the stick-slip parameter μ_{max} (Figure 6). Second, the velocity dependence of stick-slip friction changes slope at ~10 µm/s. For dry conditions, the stick-slip friction drop is independent of loading velocity for velocities ≤10 µm/s, and $\Delta\mu$ decreases with velocity above 10 µm/s (Figure 6c).

In general, for a given velocity, friction drop increases as the relative humidity increases (Figure 7a). The stick-slip friction drop is largest for the slowest velocities and the most humid conditions (Figure 7). The presence of water modulates the influence of loading rate on stick-slip stress drop, with the largest differences in $\Delta\mu$ for 1 and 100 µm/s occurring when RH = 100% (Figure 7).

3.3. Layer Thickness Evolution

We report high-resolution measurements of layer thickness (Figure 4) to assess the effects of elastoplastic contact deformation, interparticle slip and volumetric layer strain on frictional healing, and stick-slip stress drop. We note that the resolution of the DCDT used in this study (±0.1 µm), together with experiment reproducibility (Table 1), indicates that our measurements are sufficient to accurately resolve observed changes in layer thickness, which involve minimum layer dilations ≥2 µm.

We find that dilation is generally larger under the most humid conditions (Figure 7b), with the highest values of dilation observed at 100% RH. The presence of water modulates the influence of loading rate on preseismic dilation, with the largest influence of loading rate on Δh occurring under the most humid conditions (Figure 7b). For dry conditions, preseismic layer dilation is minimal and does not vary systematically with loading velocity.
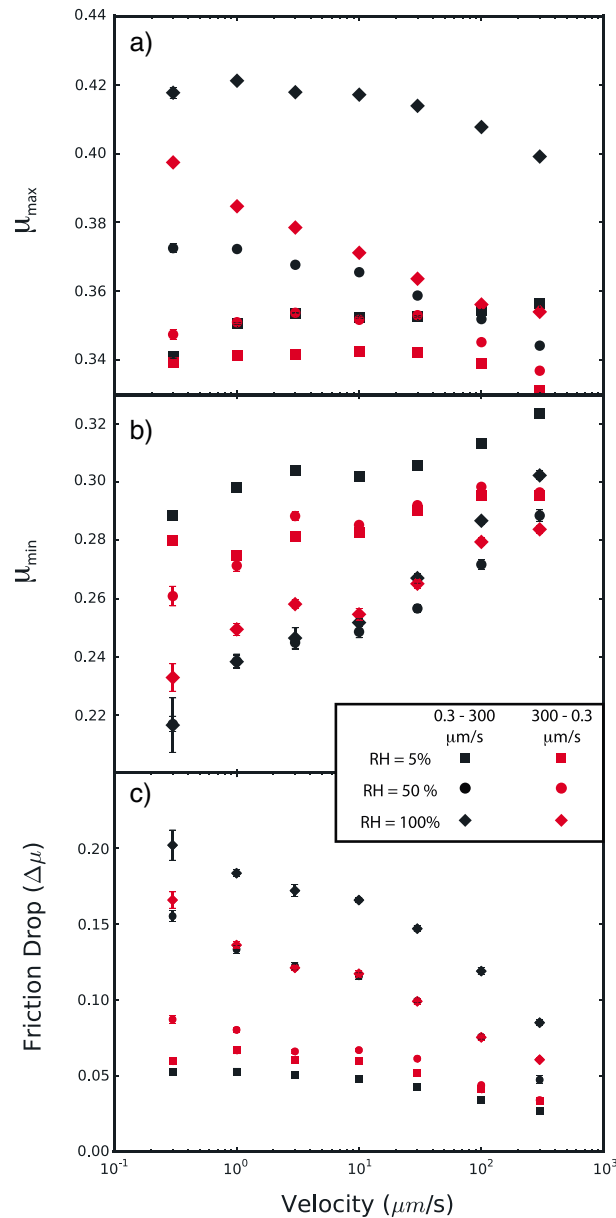
Figure 6. Stick-slip friction parameters as a function of humidity, shearing velocity, and velocity history. (a) Maximum friction, (b) minimum friction, and (c) friction drop ($\Delta\mu = \mu_{max} - \mu_{min}$) as a function of shearing velocity for each relative humidity investigated. Data points represent mean values for 20–30 stick-slip events (see Figure 5). We report the velocity sequence from 0.3 to 300 μm/s (black) and the velocity sequence from 300 to 0.3 μm/s (red) for comparison. Note that μ_{max} decreases with increasing velocity for RH ≥ 50%, but is independent of velocity for the dry cases, whereas μ_{min} increases with velocity for all the cases. Experiments in which velocity was increased during the run (0.3–300 μm/s) tend to have higher friction than experiments, in which the velocity sequence was reversed (300–0.3 μm/s). Friction drop decreases systematically with increasing shear velocity, and for runs at high RH (≥50%), the friction drop is higher when velocity was increased (0.3–300 μm/s) compared to when velocity was decreased (300–0.3 μm/s).

Loading velocity plays an important role in the evolution of layer dilation, influencing both stick-slip recurrence interval (t_r) and preseismic slip between events (Figure 8). Layer dilation increases with increasing stick-slip recurrence interval (Figure 8a), with the largest values of dilation observed for the longest t_r. The smallest values of Δh occur for the driest conditions (Figure 8). As RH increases, preseismic dilation increases to values as large as 20 μm, which corresponds to a linear strain of 0.4%. We also show that under the driest conditions, layers dilate the least and show the smallest values of preseismic slip (Figure 8b). Dilation and preseismic slip increase systematically with increasing humidity and stick-slip recurrence interval. Data from experiments at higher humidity define the same trend of dilation versus preseismic slip as those for drier conditions (Figure 8b), indicating that this trend is a property of the granular layer.

3.4. Effect of Water Content on Morphology at Grain Contact Junctions

The postdeformation SEM analysis reveals that grains are intact and do not show evidence of bulk fracture or comminution, which is consistent with expectations given that the experiments were conducted at a normal stress (5 MPa) below the grain crushing strength (Figure 9) [*Mair et al.*, 2002]. Grain-to-grain contact area and morphology are controlled strongly by the amount of water (RH) present in the system. For experiments at 5% RH, contacts are characterized by an elliptical shape and sharp rim. Additionally, contacts generally show a subrounded bulge on one side, representing plastic deformation and material pile up (Figures 9b, 9c, and 9d and Figure 13a). As relative humidity increases to 50%, contacts assume a more circular morphology characterized by (1) a well-defined rims (Figure 9f and Figure 13b), (2) a bulge with wear tracks indicating motion in one direction from the center of the contact (Figures 9f and 9g and Figure 13b), and (3) depressions that propagate from the rim toward the center of the contact (Figure 9g).

Under the most humid conditions, contact junction perimeters are almost perfectly
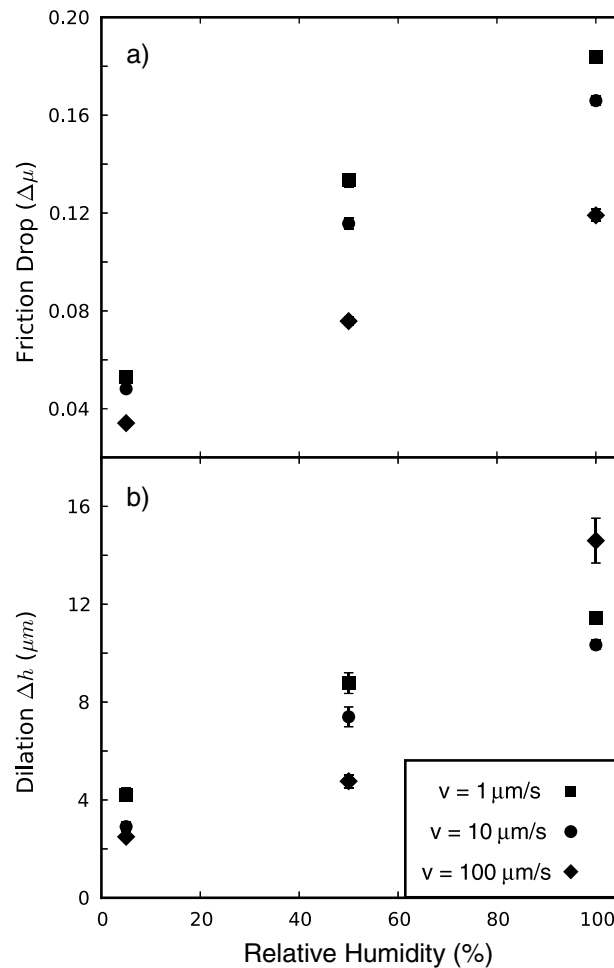
Figure 7. (a) Comparison of friction drop ($\Delta\mu$) for three different velocities (1, 10, and 100 μm/s) as a function of relative humidity for the velocity sequence 0.3 to 300 μm/s. The $\Delta\mu$ increases with increasing humidity for each shear velocity, showing the maximum values at slow velocities (i.e., longer average contact junction lifetime). (b) Evolution of preseismic dilation (Δh) as a function of relative humidity for different velocities. Dilation increases with humidity for all shearing velocities.

circular with a well-defined rim and no evidence for the bulge observed above (Figures 9l, 9m, and 9n and Figure 13c). Humid conditions also produce a more mature system of striations, than in the dry case, emerging from the center of the contact and pointing consistently in one direction (Figure 9l). Qualitatively, grain-to-grain contact area increases with increasing relative humidity (compare Figures 9d, 9h, and 9n). Unfortunately, due to the continuous changes of shear velocity throughout experiments, we cannot definitively associate a particular contact to a shear velocity, and thus, we cannot distinguish if the area observed was formed during long or short time of quasi-stationary contact between grains (i.e., recurrence time). However, during our analysis, we focused our attention on identifying the largest contacts, which likely result from the longest recurrence time.

4. Discussion

Laboratory studies and numerical simulations of frictional stick slip have proposed that water assisted chemical reactions act to restrengthen contact junctions after failure [*Rabinowicz*, 1951, 1956; *Dieterich*, 1972; *Scholz and Engelder*, 1976; *Dieterich and Conrad*, 1984; *Frye and Marone*, 2002b; *Yasuhara et al.*, 2003; *Yasuhara et al.*, 2005; *Li et al.*, 2011; *Zheng and Elsworth*, 2012, 2013]. To understand the relationship between time-dependent evolution of frictional healing and water-activated processes acting at grain junctions during the seismic cycle, we focus on the evolution of stress drop (cast in terms of friction) as a function of recurrence time, as a measure of the frictional healing rate ($\beta = \Delta\mu/\log(t_r)$). In addition, we analyze changes in layer thickness, which provide information on the role of elastoplastic deformation during aseismic creep. We combine these analyses with microscopic observations to develop a micromechanical model for shear deformation and frictional healing in granular fault gouge.

4.1. Effect of Humidity on Frictional Strength and Healing Properties of Granular Gouge Versus Bare Surfaces: Comparison With Previous Works

During the first stage of loading, we found that elastic stiffness and peak friction are influenced by the amount of water in the system. Gouges under nominally dry conditions are stiffer but weaker (smaller μ at yield) than gouges at high relative humidity. This result is in contrast with the observations of *Dieterich and Conrad* [1984] showing the opposite relation for bare quartzite surfaces, at shearing velocities of 1 μm/s and a normal stress of 1.7 MPa. Under humid conditions, they documented stick-slip instabilities and positive frictional healing, and they interpreted their results in terms of water-assisted chemical processes that induce plastic deformation and evolution of real contact area. However, in their experiments, drying the system resulted in an increase in frictional strength, suppressing time-dependent strengthening and dynamic stick
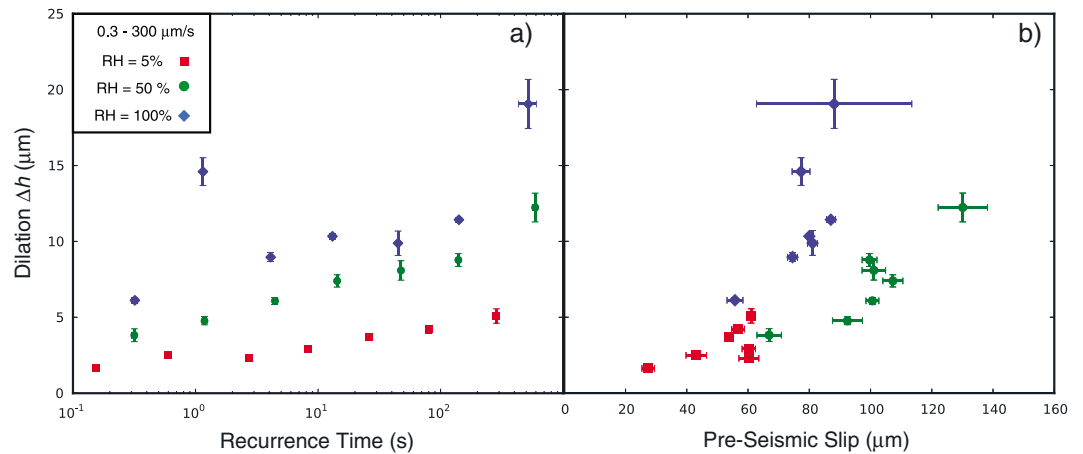
Figure 8. Granular dilation (Δh) as a function of (a) stick-slip recurrence time and (b) preseismic slip. (Figure 8a) Dilation increases with increasing recurrence time for all humidities. Maximum values of dilation are observed at 100% RH. (Figure 8b) Dilation increases with increasing preseismic slip. Runs at 100% RH show the highest values of dilation. The three experiments seem to define a single relationship between dilation and slip, with dilation increasing with increasing preseismic slip.

slip, in contrast with the results of this study. Similarly, *Renard et al.* [2012] studied the frictional aging of glass/glass flat surfaces at room temperature under dry and wet conditions. They showed that under wet conditions, and for hold times up to 3000 s, the frictional healing rate is characterized by near zero to negative values. However, drying the system caused an increase in frictional healing.

On the other hand, in accordance with our observations, *Frye and Marone* [2002b] documented an increase in frictional strength with increasing humidity in granular quartz gouge, for a range of velocities similar to those
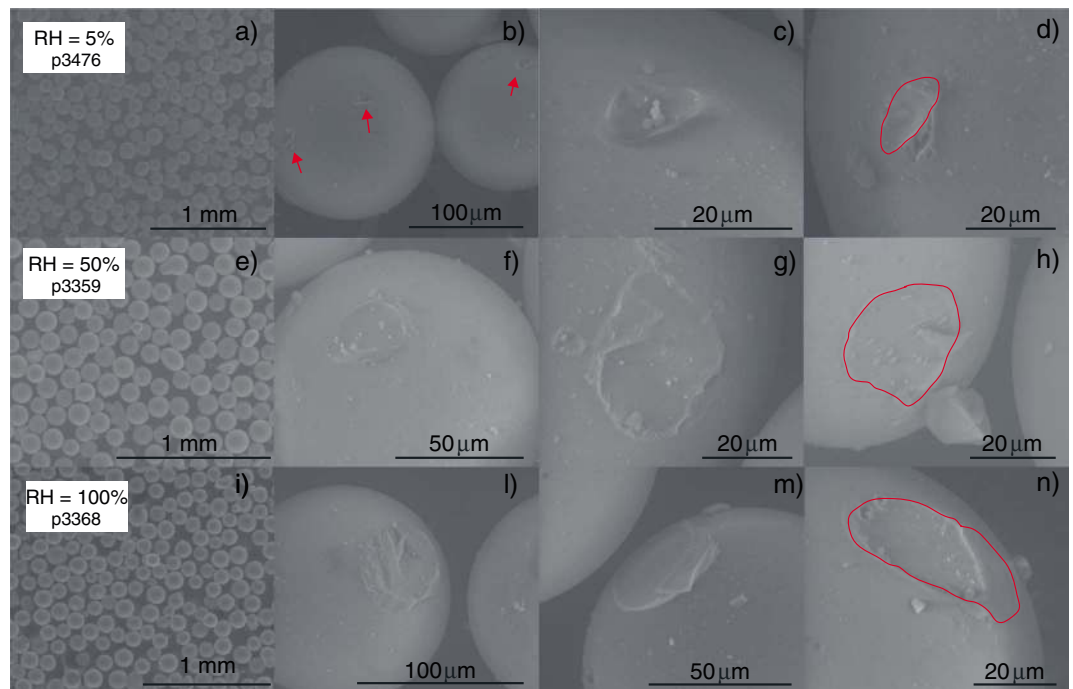

Figure 9. Postexperiment SEM images of glass beads for each RH value and at the noted magnification. (a, e, and i) The lowest magnification is shown, and beads show little evidence of bulk crushing or comminution. Details of contact junction properties can be seen for each value of RH. Note the evolution of contact junction shape from (b–d) elliptical and shallow under dry conditions to (f–h and l–n) rounded and deep with evidence of shear striations at higher RH. Contact junction size increases with increasing RH%.
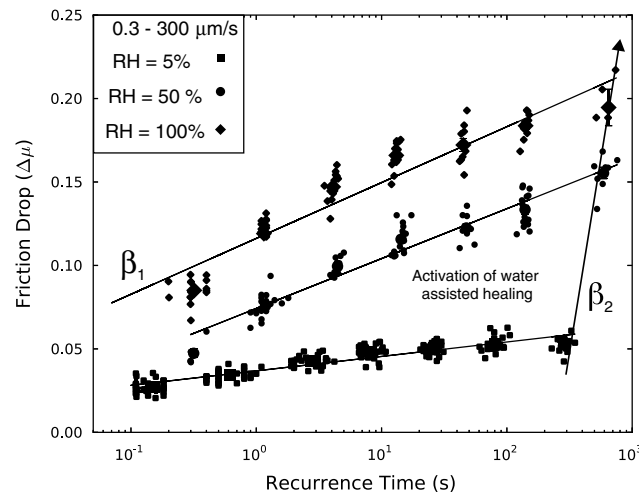
Figure 10. Stick-slip friction drop increases with recurrence time as a measure of healing rate $\beta_1 = \Delta\mu/\log(t_r)$. Note that β_1 increases from 0.014 at 5% RH ($R^2 = 0.902$) to 0.029 at 50% RH ($R^2 = 0.953$) and 0.03 at RH = 100% ($R^2 = 0.908$). For a given shearing velocity, β_2 represents the increase in friction drop and recurrence time as RH increases. The different evolution of $\Delta\mu$ with t_r highlights an activation threshold for water-assisted healing between the relative humidities of 5 and 50%.

used in our study, but at higher normal stresses. In light of these observations, we believe that the nature of the shear zone (bare surfaces versus granular gouge) is the most likely explanation for the observed differences in elastic stiffness and peak friction between bare surfaces and granular gouge.

We propose that a combination of mechanical and water-assisted processes can explain differences between the influence of humidity on friction of bare rock surfaces and granular fault gouge. Hydrolubrication at asperity contact junctions acts as a weakening mechanism on extended solid surfaces [*Roberts and Tabor*, 1970], which explains lower frictional strength of bare rock under humid conditions [*Dieterich and Conrad*, 1984; *Renard et al.*, 2012]. Water assisted, thermally activated plastic deformation processes at asperity contacts can also explain the effect of humidity on frictional

healing rate for bare rock surfaces. The growth or deformation rate of asperity contacts is low under dry conditions, which explain the observations of frictional healing for bare rock surfaces. Of course, hydrolubrication processes also operate at granular contact junctions; however, friction of granular rolling [e.g., *Marone et al.*, 2008] should be independent of interparticle contact friction, which explains the observation that steady state friction is independent of humidity for granuar gouge [*Frye and Marone*, 2002b]. On the other hand, we expect that water-assisted processes will strengthen contacts and promote shear of highly stressed interparticle contacts in force chains, which would increase the rate of frictional healing.

4.2. Frictional Healing and Its Dependence on Humidity

Shearing rate is the primary control on stick-slip frequency (i.e., recurrence time) showing an inverse power law relationship (Figure 4 inset). Our experiments show that friction drop increases logarithmically with increasing recurrence time, in agreement with a time-dependent history of contacts controlled by humidity (Figures 7 and 10). Two different rates for frictional healing emerge from our experiments: the first is associated with time-dependent evolution of contact area at grain junctions (β_1) and the second is due to elastic contact properties at grain-to-grain contacts (β_2), controlled by the amount of water available.

We observe a reduction of the frictional healing rate from $\beta_1 = 0.03$ at 100% RH, $\beta_1 = 0.029$ at 50% RH to $\beta_1 = 0.014$ at 5% RH. Gouges under humid conditions are also characterized by the largest values of preseismic dilation for the longest recurrence times (i.e., longer quasti-static contact time) and show a logarithmic decrease with t_r (Figure 8a). Preseismic dilation is nearly suppressed under dry conditions. The most likely process that induces dilation within gouges is associated with time-dependent elastoplastic deformation at grain contacts, which controls the growth of contact area [*Marone*, 1998; *Rossi et al.*, 2007; *Renard et al.*, 2012]. These observations suggest that the longer the grains are in contact, the larger the preseismic dilation (i.e., aseismic creep), during which elastoplastic deformation at grain junctions promotes granular contact growth, resulting in higher amounts of frictional healing and a larger friction drop (Figure 11).

We also observe a secondary healing mechanism (β_2) that can be attributed to the different elastic interactions between particles as RH is varied in the system (Figure 10). We report a systematic decrease in recurrence interval, dilation, and friction drop for a given shear velocity in response to a decrease in water content over the range of velocities investigated. We propose that this secondary healing mechanism is induced by drying the system, suppressing elastoplastic deformation at grain contacts and thus reducing
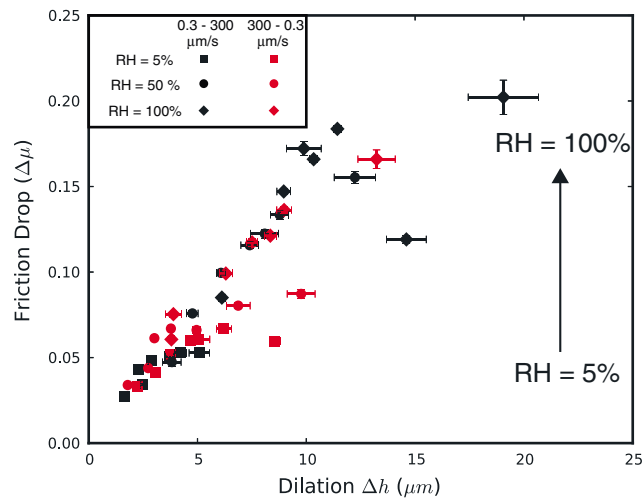
Figure 11. Relation between stick-slip friction drop and granular dilation for all humidities and velocities investigated. Note that the data for increasing velocity (0.3 to 300 μm/s) define the same trend as those for the reverse velocity sequence (300 to 0.3 μm/s). Dilation and friction drop increase with increasing relative humidity.

contact area growth. Drying of the system results in stiffer, more brittle contacts that break easier under shear compared to compliant, tougher contacts generated by plastic deformation at higher water contents. These observations suggest that time-dependent, water-activated chemical reactions act as healing mechanism at grain contacts during aseismic creep within granular gouges, controlling the evolution of grain-to-grain contact area, and can be suppressed, or strongly limited, by dry conditions.

4.3. Contact Area Growth as a Mechanism for Gouge Strengthening

Our experimental results show that an increase in relative humidity promotes gouge strengthening and increases in preseismic layer dilation (Figure 11). The observed mechanical behavior can be attributed to time-dependent, water-activated mechanisms that control the growth of grain-to-grain contact area. It has been demonstrated that the contact area at asperity junctions grows with time when gouge is under quasi-stationary contact [e.g., *Dieterich and Kilgore*, 1994; *Renard et al.*, 2012]. Time-dependent increases of asperity contact area cause the frictional resistance to shear to increase, with an increase in the overall frictional healing rate [e.g., *Marone*, 1998; *Nakatani and Scholz*, 2004]. Different processes, acting at the microscale of grain-to-grain contacts, can control the rate of contact area growth. It has been proposed that plastic deformation [e.g., *Griggs and Blacic*, 1965], contact neck growth [e.g., *Hickman and Evans*, 1991] contact neck growth and welding [e.g., *Renard et al.*, 2012], or pressure solution creep [e.g., *Niemeijer et al.*, 2008; *Gratier et al.*, 2014] are all processes that may accommodate deformation at grain-to-grain contacts, depending on the surface reactivity and pressure-temperature conditions. The availability of water in the system also plays a fundamental role in activating such processes [e.g., *Boquet et al.*, 1998; *Losert et al.*, 2000].

Our SEM postdeformation images show that grain-to-grain contact area increases as a function of relative humidity (Figures 9d, 9h, and 9n). Moreover, we report indications of pressure dissolution at high humidity, in the form of depressions propagating toward the center of the contact (Figures 9g and 9l). However, we do not observe any precipitates as indicators of recrystallization. At the end of each experimental run, when the stress field (τ and σ_n) is removed due to the granular nature of the gouge, it tends to disaggregate (Figures 9a, 9e, and 9l). During this stage, we may lose the finest particles that may characterize the recrystallization products, and as a result, we can interpret only the remanent structures on the sheared grains. Furthermore, material that precipitates during quasi-stationary contact (i.e., preseismic stage) could be destroyed during dynamic slip. The shear striations we observe on the contact surface may represent an indicator of local creep during particle rolling (i.e., aseismic creep) for gouges deformed at RH = 50 and 100% (Figures 9l and 13b). These are not observed at RH = 5%. As the applied normal stress was the same for each experiment (Table 1), we attribute the observed evolution of grain-to-grain contact area to water-activated chemical reactions that control its growth. The observation of increasing layer dilation and preseismic slip as a function of humidity also confirm that the presence of water promotes inelastic creep at grain-to-grain contacts (Figure 8b). We propose that during the aseismic creep, an increase in water availability activates time-dependent chemical reactions acting at grain contacts that promote elastoplastic deformation, leading to more contact area growth than in dry conditions. The result is a higher frictional healing rate as a function of increasing relative humidity (Figure 10). We also observe that the healing rate become nearly constant once RH = 50% is surpassed (Figure 10), suggesting a saturation threshold at which silica surfaces become completely coated with water monolayers [*Frye and Marone*, 2002b; *Asay and Kim*, 2005].
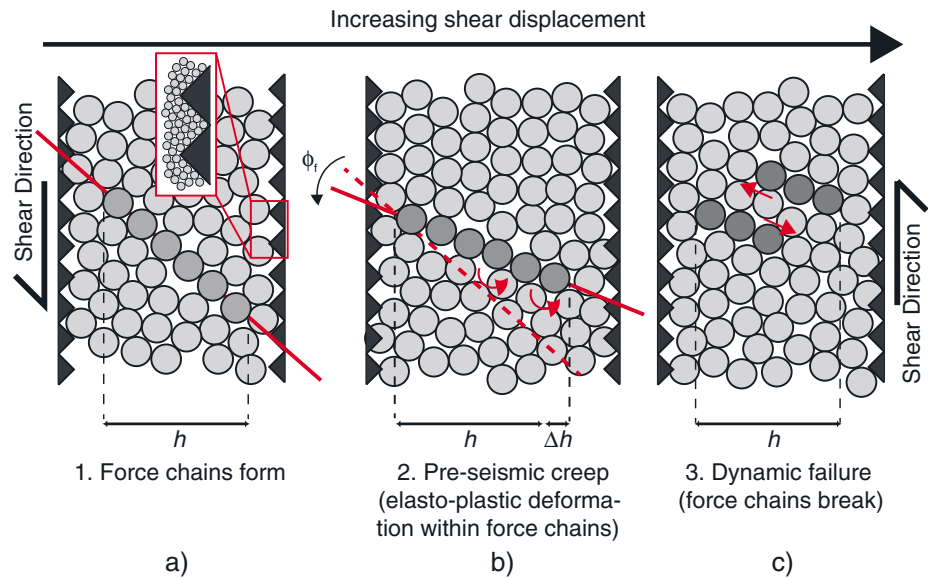
Figure 12. Schematic of deformation mechanisms during granular shear. Grains are shown larger than actual size. Shaded grains represent force chains. Note the force chains that span the layer. (a) Force chains form directly after a dynamic slip event. Inset in Figure 12a shows true scale relative to surface roughness. (b) With continuing shear, force chains deform elastoplastically due to rolling and interparticle slip, causing layer dilation. (c) Once the maximum strength and favorable orientation angle (φ_f) at grain contacts are reached, grains slide, force chains break, and dynamic failure propagate within the layer. The cycle is repeated for each stick-slip event throughout the experiment.

4.4. Micromechanical Model for Particle Contact Evolution During Shear

Particle interaction during stick-slip frictional sliding in a granular medium has been described by the continuous formation and breakage of force chains (Figure 12) [*Cundall and Strack*, 1979; *Sammis et al.*, 1987; *Morgan and Boettcher*, 1999; *Mair et al.*, 2002; *Aharonov and Sparks*, 2002; *Geng et al.*, 2003; *Anthony and Marone*, 2005; *Johnson et al.*, 2008; *Samuelson et al.*, 2009; *Tordesillas et al.*, 2012; *Griffa et al.*, 2013]. During shear loading, force concentrates along quasi-linear particle chains that carry the stress [*Majmudar and Behringer*, 2005]. Force chains are complex structures, with branches and subbranches, and are separated by spectator grains that carry little or no stress (Figure 12a). We propose that during shear, granular contacts forming force chains undergo elastoplastic deformation at the onset of preseismic slip (Figure 12b; see also Figure 4). During this stage, interparticle friction induces grain rolling until a critical shear force and a favorable orientation for sliding at particle junctions are reached [*Morgan*, 1999; *Mair et al.*, 2002]. Particle rolling results in increasing the angle between force chains and the shear zone wall, inducing macroscopic gouge layer dilation (Δh). When the critical angle for failure (φ_f) (Figure 12b) [*Mair et al.*, 2002; *Johnson et al.*, 2008] is reached and maximum shear strength is approached (μ_{max}), the particles start to slide. The result is the misalignment and breakage of force chains, leading to dynamic stick-slip failure of the entire layer, associated with abrupt compaction (Figure 12c). The load then shifts to more favorably oriented particle contacts, forming a new set of force chains, and the cycle starts over.

We posit that during the interseismic period, bonds at grain-to-grain contacts strengthen, contact area grows, and the favorable orientation for particle sliding increases as a function of increasing humidity (Figure 13). Time-dependent, water-assisted mechanisms, acting at grain contacts during shear, control the evolution of real contact area promoting plastic deformation via pressure solution processes (dissolution-precipitation) [*Hickman and Evans*, 1991, 1995; *Yasuhara et al.*, 2003; *Yasuhara et al.*, 2005; *Zheng and Elsworth*, 2012, 2013]. During quasi-stationary contact, pressure solution acts as a three-stage process: (1) dissolution at grain interfaces, (2) diffusive transport, and (3) precipitation at grain walls (Figure 14) [*Shimizu*, 1995; *Revil*, 2001; *Zheng and Elsworth*, 2012]. During preseismic slip, as water content increases, pressure solution leads to the growth of contact area and interparticle friction increases, favoring the rolling of grains, resulting in an increase of the favorable orientation for sliding (φ_f) (Figure 13).
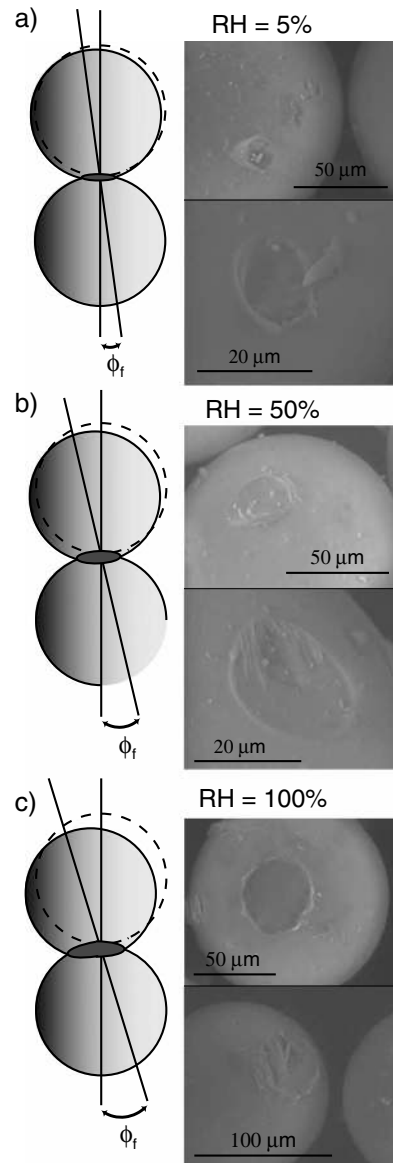
Figure 13. Comparison of contact junction deformation for different values of relative humidity. (right) SEM images and (left) a sketch for each humidity. (a) Real contact area evolution at a grain junction under relative humidity of 5%. Note the incipient contact junction associated with small interparticle shear angle (φ_f). (b) At 50% RH, the contact junction is larger due to chemically assisted mechanisms at grain junctions. Contact strength is larger, favoring rolling over sliding, which causes greater dilation until the preferred orientation for failure (φ_f) is reached. (c) At 100% RH, water at grain junctions increases pressure solution and contact growth rate, which enhances rolling and granular dilation. Grain sliding occurs at a higher interparticle friction angle, causing larger peak friction and larger stick-slip stress drop.

Our micromechanical model is supported by mechanical and postexperiment SEM observations, which show an evolution of morphology with humidity. The outer rims of contacts change from elliptical, continuous, and well defined at RH = 5% (Figure 9c and Figure 13a) to irregular with evidence of mass removal by dissolution at RH = 50 and 100% (Figures 9g and 9l) associated with a wider contact area (Figures 9d, 9h, and 9n and 13b and 13c). Our data also show that the longer the particles are in contact, and the higher the water content in the system, the larger the contact area at grain junctions and as a consequence, the larger the healing rate (β_1). During preseismic creep, increasing inelastic deformation induced by higher humidity generates more dilation via increasing the contact area at grain junctions (i.e., increase the critical angle for failure), resulting in more compliant force chains capable of storing more elastic energy and generating larger friction drops (Figure 11).

5. Conclusions

We have shown that relative humidity has a significant effect on micromechanical deformation, frictional strength, and the rate of frictional healing in granular fault gouge. We found that peak friction at yield increases and elastic stiffness decreases with increasing humidity. Our results highlight differences between the frictional properties of bare rock surfaces and granular fault gouges and, in particular, the variation in frictional strength and healing rate with relative humidity. We observed that the amount of preseismic dilation, preseismic slip, and friction drop all increase with increasing humidity and logarithmically decrease with decreasing recurrence time. We also report two different rates of frictional healing: (1) at a given humidity, stick-slip stress drop increases logarithmically with increasing recurrence time (β_1) and (2) at a given velocity, drying the system suppresses elastoplastic deformation at contact junctions, leading to an increase in elastic stiffness, which is manifested as smaller friction drops and shorter recurrence times (β_2). We report postexperiment SEM observations, which show an increase in the contact area at grain junctions with increasing humidity.

We propose a micromechanical model for granular fault gouge deformation, where time-dependent, water-assisted processes control the evolution of the contact area at grain-to-grain contacts along force chains. During preseismic slip, the increased amount of water in the system activates pressure solution processes, leading the contact area to grow with time. As a result, the longer the grains are in quasi-stationary contact, the larger the contact area, which increases interparticle friction, which promotes greater interparticle rolling. Higher interparticle friction leads to an increase of the angle for failure (φ_f) of force chains,
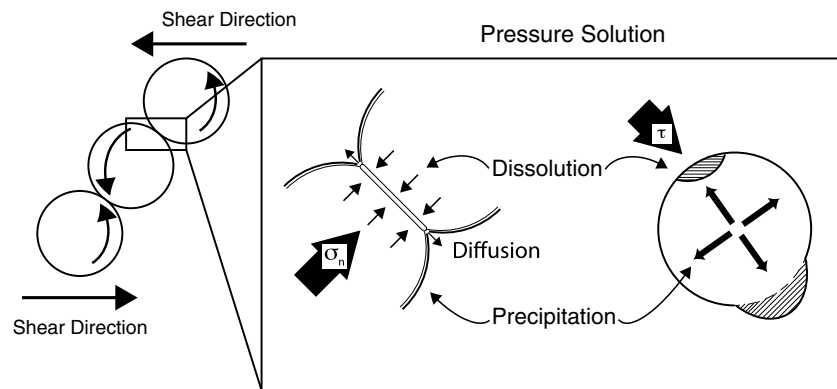
Figure 14. Schematic of chemically assisted processes at contact junctions within force chains. The sense of rolling during dilation and preseismic slip is indicated. Inset illustrates how pressure solution may occur at grain-to-grain contacts during aseismic creep. At the contact interface, stress induces dissolution, resulting in an increase in the contact area. Increased humidity enhances dissolution, favoring chemically assisted plastic deformation at contacts.

manifested in larger macroscopic layer dilation. Compliant deformation at grain-to-grain contacts within force chains, in the presence of water, results in more elastic energy stored, than in the dry case, manifesting in bigger friction drops. This mechanistic model is supported by laboratory and field observations of strength recovery on faults during the interseismic period.

References

Abe, S., and K. Mair (2005), Grain fracture in 3D numerical simulations of granular shear, *Geophys. Res. Lett.*, *32*, L05305, doi:10.1029/2004GL022123.

Abe, S., and K. Mair (2009), Effects of gouge fragment shape on fault friction: New 3D modelling results, *Geophys. Res. Lett.*, *36*, L23302, doi:10.1029/2009GL040684.

Aharonov, E., and D. Sparks (2002), Shear profiles and localization in simulations of granular materials, *Phys. Rev. E*, *65*, 051302, doi:10.1103/PhysRevE.65.051302.

Anthony, J., and C. Marone (2005), Influence of particle characteristics on granular friction, *J. Geophys. Res.*, *110*, B08409, doi:10.1029/2004JB003399.

Asay, D. B., and S. H. Kim (2005), Effects of adsorbed water layer structure on adhesion force of silicon oxide nanoasperity contact in humid ambient, *J. Chem. Phys.*, *124*, 174712, doi:10.1063/1.2192510.

Blacic, J. D., and J. M. Christie (1984), Plasticity and hydrolytic weakening of quartz single crystals, *J. Geophys. Res.*, *89*, 4223–4240.

Boquet, L., E. Charlaix, S. Ciliberto, and J. Crassous (1998), Moisture-induced ageing in granular media and the kinetics of capillary condensation, *Nature*, *396*, 735–737, doi:10.1038/25492.

Bos, B., and C. J. Spiers (2002), Fluid-assisted healing processes in gouge-bearing faults: Insights from experiments on a rock-analogue system, *Pure Appl. Geophys.*, *159*, 2537–2566.

Bos, B., C. J. Peach, and C. J. Spiers (2000), Slip behavior of simulated gouge-bearing faults under conditions favoring pressure solution, *J. Geophys. Res.*, *105*(B7), 16,699–16,717.

Brace, W. F., and J. D. Byerlee (1966), Stick-slip as a mechanism for earthquakes, *Science*, *153*(3739), 990–992.

Chester, F. M. (1994), Effects of temperature on friction: Constitutive equations and experiments with quartz gouge, *J. Geophys. Res.*, *99*, 7247–7261.

Cundall, P. A., and O. D. L. Strack (1979), A discrete numerical model for granular assemblies, *Geotechnique*, *29*, 47–65.

Dieterich, J. H. (1972), Time-dependent friction in rocks, *J. Geophys. Res.*, *77*(20), 3690–3697.

Dieterich, J. H. (1978), Time-dependent friction and the mechanics of stick-slip, *Pure Appl. Geophys.*, *116*, 790–806.

Dieterich, J. H. (1979), Modeling of rock friction, 1, Experimental results and constitutive equations, *J. Geophys. Res.*, *84*, 2161–2168.

Dieterich, J. H., and G. Conrad (1984), Effect of humidity on time and velocity dependent friction in rocks, *J. Geophys. Res.*, *89*, 4196–4202.

Dieterich, J. H., and B. D. Kilgore (1994), Direct observation of frictional contacts: New insights for state-dependent properties, *Pure Appl. Geophys.*, *143*(1/2/3), 283–302.

Frye, K. M., and C. Marone (2002a), The effect of particle dimensionality on granular friction in laboratory shear zones, *Geophys. Res. Lett.*, *29*(19), 1916, doi:10.1029/2002GL015709.

Frye, K. M., and C. Marone (2002b), Effect of humidity on granular friction at room temperature, *J. Geophys. Res.*, *107*(B11), 2309, doi:10.1029/2001JB000654.

Geng, J., G. Reydellet, E. Clément, and R. P. Behringer (2003), Green's function measurements of force transmission in 2D granular materials, *Physica D*, *182*, 274–303, doi:10.1016/S0167-2789(03)00137-4.

Gratier, J.-P., F. Renard, and B. Vial (2014), Postseismic pressure solution creep: Evidence and time-dependent change from dynamic indenting experiments, *J. Geophys. Res. Solid Earth*, *119*, doi:10.1002/2013JB010768.

Griffa, M., B. Ferdowsi, R. A. Guyer, E. G. Daub, P. A. Johnson, C. Marone, and J. Carmeliet (2013), Influence of vibration amplitude on dynamic triggering of slip in sheared granular layers, *Phys. Rev. E*, *87*, 012205, doi:10.1103/PhysRevE.87.012205.

Griggs, D. T., and J. D. Blacic (1965), Quartz: Anomalous weakness of synthetic crystals, *Science*, *147*(3655), 292–295.

Guo, Y., and J. K. Morgan (2004), Influence of normal stress and grain shape on granular friction: Results of discrete element simulation, *J. Geophys. Res.*, *109*, B12305, doi:10.1029/2004JB003044.

Guo, Y., and J. K. Morgan (2006), The frictional and micromechanical effects of grain comminution in fault gouge from distinct element simulations, *J. Geophys. Res.*, *111*, B12406, doi:10.1029/2005JB004049.

Hickman, S. H., and B. Evans (1991), Experimental Pressure Solution in Halite, 1: The effect of grain/interphase boundary structure, *J. Geol. Soc. London*, *148*, 549–560.

Hickman, S. H., and B. Evans (1995), Kinetics of pressure solution at halite-silica interfaces and intergranular clay films, *J. Geophys. Res.*, *100*, 13,113–13,132.

Johnson, P. A., H. Savage, M. Knuth, J. Gomberg, and C. Marone (2008), Effects of acoustic waves on stick-slip in granular media and implications for earthquakes, *Nature*, *451*, 57–60, doi:10.1038/nature06440.

Johnson, P. A., B. Ferdowsi, B. M. Kaproth, M. Scuderi, M. Griffa, J. Carmeliet, R. A. Guyer, P.-Y. Le Bas, D. T. Trugman, and C. Marone (2013), Acoustic emission and microslip precursors to stick-slip failure in sheared granular material, *Geophys. Res. Lett.*, *40*, 5627–5631, doi:10.1002/2013GL057848.

Kanamori, H., and C. R. Allen (1986), in *Earthquake repeat time and average stress drop*, *Geophys. Monogr. Ser.*, vol. 37, edited by S. Das, J. Boatwright, and C. H. Scholz, pp. 227–236, AGU, Washington, D. C.

Karner, S. L., and C. Marone (2000), Effects of loading rate and normal stress on stress drop and stickslip recurrence interval, in *Geocomplexity and the Physics of Earthquakes*, *Geophys. Monogr. Ser.*, vol. 120, edited by J. B. Rundle, D. L. Turcotte, and W. Klein, pp. 187–198, AGU, Washington, D. C.

Li, Q., T. E. Tullis, D. Goldsby, and R. W. Carpick (2011), Frictional ageing from interfacial bonding and the origins of rate and state friction, *Nature*, *480*, 233–236, doi:10.1038/nature10589.

Losert, W., J.-C. Geminard, S. Nansuno, and J. P. Gollub (2000), Mechanisms for slow strengthening in granular materials, *Phys. Rev. E*, *61*, 4060.

Mair, K., and S. Abe (2008), 3D numerical simulations of fault gouge evolution during shear: Grain size reduction and strain localization, *Earth Planet. Sci. Lett.*, *274*, 72–81.

Mair, K., and S. Abe (2011), Breaking up: Comminution mechanisms in sheared simulated fault gouge, *Pure Appl. Geophys.*, *168*, 2277–2288, doi:10.1007/s00024-011-0266-6.

Mair, K., K. M. Frye, and C. Marone (2002), Influence of grain characteristics on the friction of granular shear zones, *J. Geophys. Res.*, *107*(B10), 2219, doi:10.1029/2001JB000516.

Majmudar, T., and R. P. Behringer (2005), Contact forces and stress-induced anisotropy in granular materials, *Nature*, *435*, 1079–1082, doi:10.1038/nature03805.

Marone, C. (1998), Laboratory-derived friction laws and their application to seismic faulting, *Annu. Rev. Earth Planet. Sci.*, *26*, 643–696.

Marone, C., J. E. Vidale, and W. Ellsworth (1995), Fault healing inferred from time dependent variations in source properties of repeating earthquakes, *Geophys. Res. Lett.*, *22*, 3095–3098.

Marone, C., B. M. Carpenter, and P. Schiffer (2008), Transition from rolling to jamming in thin granular layers, *Phys. Rev. Lett.*, *101*, 248001, doi:10.1103/PhysRevLett.101.248001.

Mora, P., and D. Place (1994), Simulation of the frictional stick-slip instability, *Pure Appl. Geophys.*, *143*, 61–87.

Mora, P., and D. Place (1998), Numerical simulation of earthquake faults with gouge: Toward a comprehensive explanation for the heat flow paradox, *J. Geophys. Res.*, *103*, 21,067–21,089.

Mora, P., and D. Place (1999), The weakness of earthquake faults, *Geophys. Res. Lett.*, *26*, 123–126.

Morgan, J. K. (1999), Numerical simulations of granular shear zones using the distinct element method, 2, Effects of particle size distribution and interparticle friction on mechanical behavior, *J. Geophys. Res.*, *104*, 2721–2732.

Morgan, J. K., and M. S. Boettcher (1999), Numerical simulations of granular shear zones using the distinct element method, 1, Shear zone kinematics and the micromechanics of localization, *J. Geophys. Res.*, *104*, 2703–2719.

Nakatani, M., and C. H. Scholz (2004), Frictional healing of quartz gouge under hydrothermal conditions: 1. Experimental evidence for solution transfer healing mechanism, *J. Geophys. Res.*, *109*, B07201, doi:10.1029/2001JB001522.

Niemeijer, A., C. Marone, and D. Elsworth (2008), Healing of simulated fault gouges aided by pressure solution: Results from rock analogue experiments, *J. Geophys. Res.*, *113*, B04204, doi:10.1029/2007JB005376.

Niemeijer, A., C. Marone, and D. Elsworth (2010), Frictional strength and strain weakening in simulated fault gouge: Competition between geometrical weakening and chemical strengthening, *J. Geophys. Res.*, *115*, B10207, doi:10.1029/2009JB000838.

Niemeijer, A. R., C. J. Spiers, and B. Bos (2002), Compaction creep of quartz sand at 400-600 °C: Experimental evidence for dissolution-controlled pressure solution, *Earth Planet. Sci. Lett.*, *195*, 261–275.

Peng, Z., J. E. Vidale, C. Marone, and A. Rubin (2005), Systemic variations in recurrence interval and moment of repeating aftershocks, *Geophys. Res. Lett.*, *32*, L15301, doi:10.1029/2005GL022626.

Rabinowicz, E. (1951), The nature of static and kinetic coefficients of friction, *J. Appl. Phys.*, *22*, 1373–1379.

Rabinowicz, E. (1956), Stick and Slip, *Sci. Am.*, *194*(5), 109–119, doi:10.1038/scientificamerican0556-109.

Rathbun, A. P., F. Renard, and S. Abe (2013), Numerical investigation of the interplay between wall geometry and friction in granular fault gouge, *J. Geophys. Res. Solid Earth*, *118*, 878–896, doi:10.1002/jgrb.50106.

Renard, F., S. Beaupretre, C. Voisin, D. Zigone, T. Candela, D. K. Dysthe, and J. P. Gratier (2012), Strength evolution of a reactive frictional interface is controlled by the dynamics of contacts and chemical effects, *Earth Planet. Sci. Lett.*, *341–344*, 20–34, doi:10.1016/j.epsl.2012.04.048.

Revil, A. (2001), Pervasive pressure solution transfer in a quartz sand, *J. Geophys. Res.*, *106*, 8665–8686.

Roberts, A. D., and D. Tabor (1970), Mechanical properties of very thin surface films, *Spec. Discuss. Faraday Soc.*, *1*, 243–250, doi:10.1039/SD9700100243.

Rossi, M., O. Vidal, B. Wunder, and F. Renard (2007), Influence of time, temperature, confining pressure and fluid content on the experimental compaction of spherical grains, *Tectonophysics*, *441*, 47–65, doi:10.1016/j.tecto.2007.05.001.

Ruina, A. (1983), Slip instability and state variable friction laws, *J. Geophys. Res.*, *88*, 10,359–10,370.

Sammis, C., G. King, and R. Biegel (1987), The kinematics of gouge deformation, *Pure Appl. Geophys.*, *125*(5), 777–812.

Samuelson, J., D. Elsworth, and C. Marone (2009), Shear-induced dilatancy of fluid-saturated faults: Experiment and theory, *J. Geophys. Res.*, *114*, B12404, doi:10.1029/2008JB006273.

Savage, H. M., and C. Marone (2007), Effects of shear velocity oscillations on stick-slip behavior in laboratory experiments, *J. Geophys. Res.*, *112*, B02301, doi:10.1029/2005JB004238.

Savage, H. M., and C. Marone (2008), Potential for earthquake triggering from transient deformation, *J. Geophys. Res.*, *113*, B05302, doi:10.1029/2007JB005277.

Schaff, D. P., G. C. Beroza, and B. E. Shaw (1998), Postseismic response of repeating aftershocks, *Geophys. Res. Lett.*, *25*, 4549–4552.

Scholz, C. H. (2002), *The Mechanics of Earthquakes and Faulting*, 2nd ed., Cambridge Univ. Press, New York.

Scholz, C. H., and J. T. Engelder (1976), The role of asperity indentation and ploughing in rock friction, I, Asperity creep and stick-slip, *Int. J. Rock Mech. Min. Sci.*, *13*, 149–154.

Scholz, C. H., C. A. Aviles, and S. G. Wesnousky (1986), Scaling differences between large interplate and intraplate earthquakes, *Bull. Seismol. Soc. Am.*, *76*, 65–70.

Scott, D. R., C. Marone, and C. G. Sammis (1994), The apparent friction of granular fault gouge in sheared layers, *J. Geophys. Res.*, *99*(B4), 7231–7246.

Shimizu, I. (1995), Kinetics of pressure solution creep in quartz: Theoretical considerations, *Tectonophysics*, *245*, 121–134.

Tenthorey, E., and S. Cox (2006), Cohesive strengthening of fault zones during the interseismic period: An experimental study, *J. Geophys. Res.*, *111*, B09202, doi:10.1029/2005JB004122.

Teufel, L. W., and J. M. Logan (1978), Effect of displacement rate on the real area of contact and temperatures generated during frictional sliding of Tennessee sandstone, *Pure Appl. Geophys.*, *116*, 840–865.

Tordesillas, A., D. M. Walker, G. Froyland, J. Zhang, and R. P. Behringer (2012), Transition Dynamics of Frictional Granular Clusters, *Phys. Rev, E*, *86*, 011306.

Tullis, T. E. (1988), Rock friction constitutive behavior from laboratory experiments and its implications for an earthquake prediction field monitoring program, *Pure Appl. Geophys.*, *126*, 555–588.

Tullis, T. E., and J. D. Weeks (1986), Constitutive behavior and stability of frictional sliding of granite, *Pure Appl. Geophys.*, *124*, 383–414.

Vidale, J. E., W. L. Ellsworth, A. Cole, and C. Marone (1994), Variations in rupture processes with recurrence interval in a repeated small earthquake, *Nature, 368*, 624–626.

Visser, H. J. M., C. J. Spiers, and S. J. T. Hangx (2012), Effects of interfacial energy on compaction creep by intergranular pressure solution: Theory vs. experiments on a rock analogue (NaNO3), *J. Geophys. Res.*, *117*, B11211, doi:10.1029/2012JB009590.

Yasuhara, H., C. Marone, and D. Elsworth (2005), Fault zone restrengthening and frictional healing: The role of pressure solution, *J. Geophys. Res.*, *110*, B06310, doi:10.1029/2004JB003327.

Yasuhara, H., D. Elsworth, and A. Polak (2003), A mechanistic model for compaction of granular aggregates moderated by pressure solution, *J. Geophys. Res.*, *108*(B11), 2530, doi:10.1029/2003JB002536.

Zhang, X. M., and C. J. Spiers (2005), Compaction of granular calcite by pressure solution at room temperature and effects of pore fluid chemistry, *Int. J. Rock Mech. Min. Sci.*, *42*, 950–960.

Zheng, B., and D. Elsworth (2012), Evolution of permeability in heterogeneous granular aggregates during chemical compaction: Granular mechanics models, *J. Geophys. Res.*, *117*, B03206, doi:10.1029/2011JB008573.

Zheng, B., and D. Elsworth (2013), Strength evolution in heterogeneous granular aggregates during chemo-mechanical compaction, *Int. J. Rock Mech. Min. Sci.*, *60*, 217–226, doi:10.1016/j.ijrmms.2012.12.031.